Competing mechanisms for step meandering in unstable growth

Jouni Kallunki and Joachim Krug

Fachbereich Physik, Universität Essen, 45117 Essen, Germany

Miroslav Kotrla

Institute of Physics, Academy of Sciences of the Czech Republic, Na Slovance 2, 182 21 Prague 8, Czech Republic

The meander instability of a vicinal surface growing under step flow conditions is studied within a solid-on-solid model. In the absence of edge diffusion the selected meander wavelength agrees quantitatively with the continuum linear stability analysis of Bales and Zangwill [Phys. Rev. B **41**, 4400 (1990)]. In the presence of edge diffusion a local instability mechanism related to kink rounding barriers dominates, and the meander wavelength is set by one-dimensional nucleation. The long-time behavior of the meander amplitude differs in the two cases, and disagrees with the predictions of a nonlinear step evolution equation [O. Pierre-Louis *et al.*, Phys. Rev. Lett. **80**, 4221 (1998)]. The variation of the meander wavelength with the deposition flux and with the activation barriers for step adatom detachment and step crossing (the Ehrlich-Schwoebel barrier) is studied in detail. The interpretation of recent experiments on surfaces vicinal to Cu(100) [T. Maroutian *et al.*, Phys. Rev. B **64**, 165401 (2001)] in the light of our results yields an estimate for the kink rounding barrier at the close-packed steps.

I. INTRODUCTION

It has been shown in several experiments and computer simulations that during epitaxial growth on a vicinal crystal surface, straight steps are unstable against the formation of an in-phase meander.[1,2] The phenomenon was first predicted theoretically by Bales and Zangwill (BZ) within a continuum theory.[3] According to BZ, step meandering is caused by an energy barrier, the Ehrlich-Schwoebel (ES) barrier,[4] which suppresses the attachment of surface atoms to the step from the terrace above. The preferential attachment from below implies that protrusions in the step are amplified, leading to a linear diffusional instability.

Recent experimental measurements of the meander wavelength on vicinal copper surfaces[5,6] showed significant disagreement with the predictions of the BZ theory. This has led to a search for alternative sources of instability.[7–9] The most prominent alternative mechanism is the kink Ehrlich-Schwoebel effect (KESE), which invokes a kinetic barrier that prevents atoms diffusing along step edges to cross corners or kinks.[10–12] In close analogy to the ES instability of singular crystal surfaces,[13–15] this induces a destabilizing mass current along the step.

In this article we present kinetic Monte Carlo (KMC) simulations of step meandering which display both types of instabilities within a single model. The relative importance of the KESE vs the BZ instability can be tuned through the facility of step-edge diffusion. By explicitly relating the parameters of the KMC model to those of the continuum theory, we show that the meander wavelength can be quantitatively predicted in both instability regimes. Our study thus proves the feasibility of extracting kinetic barriers from experimental meander morphologies. The simulations also provide some insight into the long-time behavior of the meander amplitude, which can be compared to the predictions of nonlinear continuum equations.[16–18]

The model employed in our work is described in Sec. II. Section III summarizes the predictions of continuum theory for the meander wavelength, and explains how the material parameters of the continuum description are determined for the KMC model. The simulation results are presented in Sec. IV. We provide some discussion of the applicability of the KESE scenario to the experiments[6] on Cu(100) in Sec. V, and conclude in Sec. VI.

II. MODEL

We employ a standard solid-on-solid (SOS) model,[19] in which the crystal surface is represented by columns of integer height $h_{\mathbf{r}}$ on a square lattice of substrate sites $\mathbf{r}$. The elementary processes are the deposition of atoms at rate F and the hopping of adatoms to nearest-neighbor sites with a rate

$$r = r_0 \exp(-E_a/k_B T). \tag{1}$$

The activation barrier E_a depends on the local configuration through

$$E_a = E_S + n_i E_n + (n_i - n_f)\Theta(n_i - n_f)E_{BB} \\ + (m_i - m_f)\Theta(m_i - m_f)E_{ES}, \tag{2}$$

where E_S is the energy barrier for diffusion on a flat terrace, E_n is the contribution of a nearest-neighbor bond to the energy barrier, E_{BB} is an additional energy cost for bond breaking, and E_{ES} is the ES barrier; n_i denotes the number of in-plane nearest neighbors before the hop and n_f after the hop, while m_i and m_f are the number of next-nearest neighbors in the planes beneath and above before (m_i) and after (m_f) the hop. The Heaviside function $\Theta(x) = 1$ if $x > 0$, and 0 otherwise.

The implementation of the ES barrier through the change in the number of out-of-plane next-nearest neighbors has
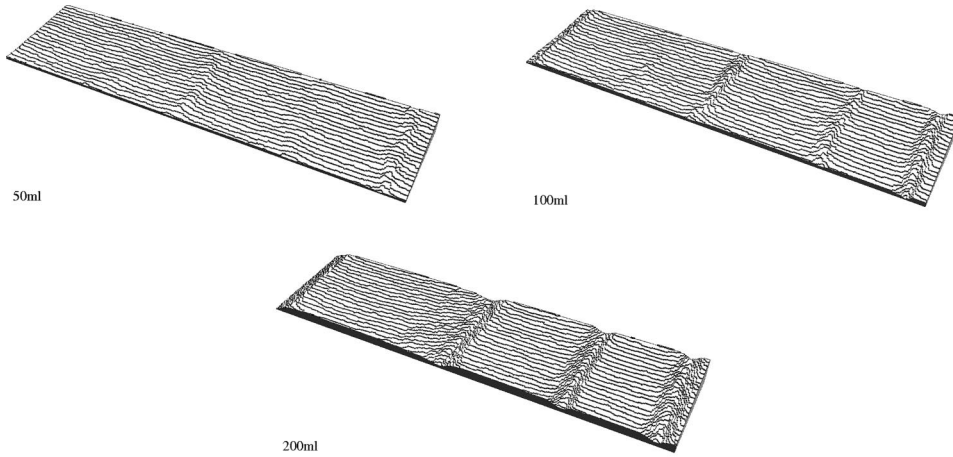
FIG. 1. Evolution of a vicinal surface with initially straight steps under the dynamics of model I. Snapshots show a 120×500 piece of a larger system (120×1000 with 20 steps) after deposition of 50, 100, and 200 ML. The deposition flux was $F=0.2$ ML/s, and the other parameters are as described in the text.

been used in several earlier growth studies,[2,20,21] and the additional bond breaking energy E_{BB} was introduced in the context of ion sputtering.[22] The rates defined by Eqs. (1) and (2) satisfy detailed balance with respect to the Hamiltonian:

$$H=\sum_{\langle\mathbf{r},\mathbf{r}'\rangle}[E_K|h_{\mathbf{r}}-h_{\mathbf{r}'}|+E_{ES}(|h_{\mathbf{r}}-h_{\mathbf{r}'}|-1)$$
$$\times\Theta(|h_{\mathbf{r}}-h_{\mathbf{r}'}|-1)]. \qquad (3)$$

The sum runs over all nearest-neighbor pairs, and

$$E_K=\tfrac{1}{2}(E_n+E_{BB}) \qquad (4)$$

is the energy per unit length of a single height step running along one of the lattice axes; for the SOS model, this is also the kink energy. The detailed balance condition is easily checked by noting that the rates can be written as a product of Arrhenius [the term proportional to E_n in Eq. (2)] and Metropolis (terms proportional to E_{BB} and E_{ES}) dynamics,[21] each of which fulfill detailed balance with respect to part of the Hamiltonian (3).

Setting $E_{BB}=0$ the model, called hereafter *model I*, does not include diffusion along the step edges, because the hopping rate along the step is equal to the rate of detachment from the step. Edge diffusion is facilitated compared to detachment if $E_{BB}>0$ (hereafter called *model II*). Model II also

contains a kink ES barrier, since atoms cannot round corners without detaching from the edge.

The simulations were carried out on rectangular lattices with periodic boundary conditions in the step direction and helical boundary conditions in the direction of the vicinality. The initial step spacing was typically $l=6$ (exceptions are noted in the figure captions). For both models the values for the activation barriers were set to $E_S=0.35$ eV, $E_n=0.21$ eV and $E_{ES}=0.15$ eV, $E_{BB}=0$ for model I and for model II we put $E_{BB}=E_n=0.21$ eV. The temperature was $T=375$ K, the diffusion prefactor $r_0=2\times10^{11}$ s^{-1} ($r_0=4\times10^{12}$ s^{-1}) for model I (model II), and the deposition flux was varied in the range $F=0.005-1.0$ ML/s. These choices were motivated mainly by our desire to study the variation of the meander wavelength over a range of control parameters without being strongly affected by finite-size effects and limited computer time. In particular, the different diffusion prefactors for the two models were chosen only to be able to study both models in the same range of flux and temperature, and do not carry any physical significance.

Typical configurations generated in the simulations are shown in Figs. 1, 2, and 3. For both models the initially straight steps form an in-phase meander pattern with a characteristic wavelength. The selected wavelength remains constant during growth. The dependence of the meander wavelength on the model parameters is the main focus of the
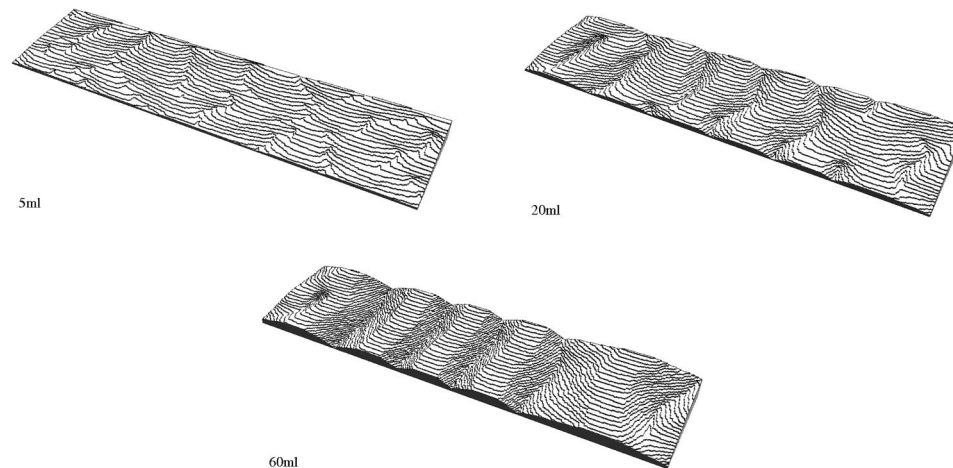

FIG. 2. Evolution under the dynamics of model II. Snapshots show a 120×500 piece of a larger system (120×800 with 20 steps) after deposition of 5, 20, and 60 ML. The deposition flux was $F=0.01$ ML/s, and the other parameters are as described in the text.
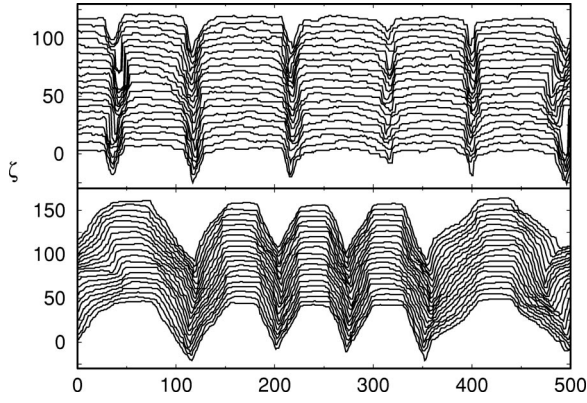
FIG. 3. Step configurations for models I (upper panel) and II (lower panel) after deposition of 75 ML at a deposition flux $F = 0.5$ ML/s (model I) and $F = 0.01$ ML/s (model II). The figures show part of a 800×120 lattice with 20 steps.

following discussion. Some aspects of the temporal evolution of the pattern will be addressed in Sec. IV D.

III. RELEVANT LENGTH SCALES

Before turning to the quantitative analysis of the simulations, we summarize the available theoretical predictions for the length scale of the meander instability.

A. Bales-Zangwill instability

The BZ analysis proceeds by solving a diffusion equation for the adatom concentration with boundary conditions given by the attachment-detachment kinetics at the steps. It predicts an in-phase meander[23] with a dominant wavelength[18]

$$\lambda_{BZ} = 4\pi \sqrt{\frac{\Gamma(\Omega l D c_{eq}^0 + a\sigma_{st})}{\Omega f_S F l^2}}. \tag{5}$$

Here Ω denotes the atomic area and a is the lattice spacing. All kinetic and thermodynamic parameters entering Eq. (5) can be expressed in terms of the microscopic rates and energies of the KMC model. The diffusion coefficient on the terrace reads $D = r_0 \exp(-E_S/k_B T)$, and the step edge stiffness is given by[24] $\Gamma = 2a \sinh^2(E_K/2k_B T)$. To calculate the equilibrium adatom concentration c_{eq}^0 and the mobility σ_{st} along the step edge, it is useful to consider the step as a one-dimensional (1D) SOS interface in equilibrium with the adatom gas on the terrace. For model I the transition rates are of Arrhenius form, i.e., dependent only on the configuration before the jump, and exact results for c_{eq}^0 and σ_{st} can be found.[25] We obtain $c_{eq}^0 = \exp(-2E_n/k_B T)$ and $\sigma_{st} = (D/2)\exp(-2E_n/k_B T)$.

For model II the transition rates are no longer of Arrhenius type, and the exact results[25] cannot be directly applied. Within linear fluctuation theory, the step edge mobility has been estimated as $\sigma_{st} = a^2/\tau_L$, where τ_L is the characteristic time for detachment from a kink.[26] For our model II this yields

$$\sigma_{st} \approx D \exp[-(2E_n + E_{BB})/k_B T]. \tag{6}$$

Strictly speaking, Eq. (6) has to be modified in the presence of kink ES barriers which reduce mass transport along the edge. A detailed analysis[27] shows that an additional KESE barrier E_{KES} becomes relevant when $E_{KES} > E_K$. In our simulations $E_{KES} \approx E_{BB} \lesssim E_K$ always, so Eq. (6) suffices. The terrace adatom concentration is generally given by the expression $c_{eq}^0 = \exp(-\Delta E/k_B T)$, where $\Delta E = 4E_K$ is the formation energy for moving an adatom from a kink to the terrace.[28]

The strength of the ES effect is contained in the parameter $f_S = (l_- - l_+)/(l + l_- + l_+)$, where the length scales[14,28] $l_\pm = D/k_\pm$ are inversely proportional to the attachment rates for adatoms approaching the step from below (k_+) or above (k_-) (l_- is also known[15] as the ES length l_{ES}). For the KMC model we estimate

$$k_+ = D, \quad k_- \approx D\exp(-E_{ES}/k_B T). \tag{7}$$

In fact the rate of attachment from the upper terrace depends on the microscopic configuration of the step. A direct test of relation (7) is presented below in Sec. IV C.

The expression used above for the edge mobility σ_{st} is valid only on length scales longer than the kink distance $l_K \approx (1/2)\exp(E_K/k_B T)$. On shorter scales edge diffusion is much more efficient, and the expression for the characteristic meander wavelength must be replaced by[9]

$$\tilde{\lambda}_{BZ} = 2^{1/4}\sqrt{l_K\pi}\lambda_{BZ}^{1/2} \tag{8}$$

when edge diffusion dominates and $l_K \gg \lambda_{BZ}$.

B. KESE instability

Step meandering due to the KESE can be discussed[10] in analogy to the ES instability of a one-dimensional surface.[13,15] The characteristic wavelength depends on the one-dimensional *nucleation length* l_D, which is defined as the average distance between two dimers that are nucleated on a straight step at the beginning of deposition, and the kink ES length $l_{KES} \approx \exp[E_{KES}/k_B T]$. For a strong KESE, in the sense that $l_D \ll l_{KES}$, the initial meander wavelength is l_D, while for a weak KESE ($l_D \gg l_{KES}$) it is of the order of[13,14]

$$\lambda_w \approx (l_D/l_{KES})^{1/2}l_D. \tag{9}$$

From one-dimensional nucleation theory the expression

$$l_D = (12D_{st}/Fl)^{1/4} \tag{10}$$

for the nucleation length can be derived;[29] here Fl is the flux of terrace atoms onto the step. In contrast to the mobility σ_{st}, the edge diffusion coefficient D_{st} refers to the motion of an edge atom along a *straight* step without kinks, and is given by $D_{st} = D\exp(-E_n/k_B T)$ in the SOS model.

It should be noted that Eqs. (9) and (10) apply to a 1D surface in the absence of desorption; for a step this translates into neglecting the detachment from the step. This approximation clearly breaks down as the bond breaking barrier E_{BB} approaches zero. Including the detachment from the step introduces a new length scale into the problem, namely, the diffusion length $x_s = \sqrt{D_{st}\tau}$. Here τ is the time an adatom diffuses along a straight step before being ''evaporated'' to
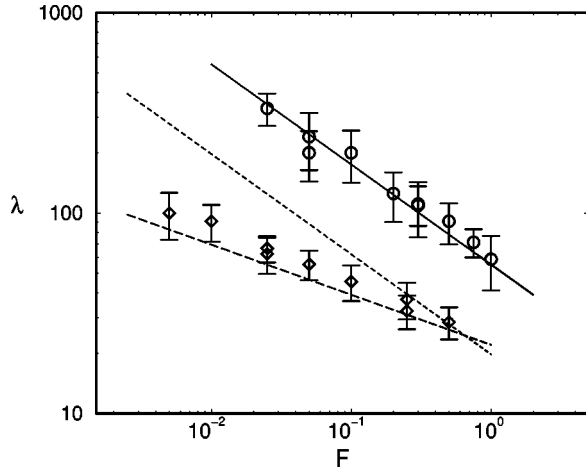
FIG. 4. Meander wavelength as a function of flux for models I (circles) and II (diamonds). Each symbol represents a single run on a lattice of size 1000×30 with five steps. The error bars refer to the variation of the wavelength within the configuration. For some fluxes results for a lattice of size 1200×30 have also been included. The simulations were run until the meander wavelength was clearly visible. The BZ length [Eq. (5)] is plotted as a full line for model I and a short-dashed line for model II. The long-dashed line is the nucleation length [Eq. (10)] for model II.

the terrace, and x_s the distance the atom travels along the step in time interval τ. A lower bound for τ is given by the detachment rate from the straight step $\tau^{-1} = D_{st} \exp(-E_{BB}/k_B T)$. In reality detached atoms have a high probability of reattachment, and thus the real evaporation time τ is longer. A lower bound for the diffusion length then reads $x_s = \exp(E_{BB}/2k_B T)$. Repeating the calculation of the nucleation length for a 1D surface with desorption,[27] one arrives at an expression for the nucleation length in the limit $x_s \ll l_D$, which reads

$$l_D = \left(\frac{D_{st}}{Fl}\right)^{1/2} \frac{1}{x_s}. \qquad (11)$$

The same result can also be obtained by applying the scaling arguments of Jensen *et al.*[30] in one dimension. For general values of x_s, l_D is given as the solution of a transcendental equation. A simple expression interpolating between the two cases (10) and (11) reads

$$l_D = \left(\frac{D_{st}}{Fl}\right)^{1/4} \left[12^{1/4} + \frac{1}{x_s}\left(\frac{D_{st}}{Fl}\right)^{1/4}\right]. \qquad (12)$$

In the case of a weak KESE, repeating the calculation of Politi and Villain[13] with desorption, one finds[27] that for $x_s \ll l_{KES} \ll l_D$ the most unstable wavelength is of the order

$$\lambda_w \approx l_D^2/x_s, \qquad (13)$$

which replaces Eq. (9).

IV. SIMULATION RESULTS

A. Meander mechanisms

Figure 4 shows the meander wavelength as a function of

deposition flux obtained from our KMC simulations. The wavelength was extracted from the profiles directly by measuring the distance between subsequent minima in a single profile. The error bars refer to the variation of the wavelength within a single profile. For model I the wavelength is found to scale as $F^{-0.47 \pm 0.06}$, in qualitative agreement with both the BZ length λ_{BZ} and the nucleation length l_D in the detachment-dominated limit [Eq. (11); for model I, $x_s \approx 1 \ll l_D$]. Quantitatively the results are found to agree with λ_{BZ} for the parameters used in the simulations, while the nucleation length l_D is smaller by approximately a factor 1/2. A more convincing piece of evidence for the Bales-Zangwill mechanism is the dependence of the meander wavelength on the Ehrlich-Schwoebel barrier E_{ES}, which is discussed below in Sec. IV C. The nucleation length is obviously independent of E_{ES}.

For model II the meander wavelength scales as $F^{-0.28 \pm 0.05}$, which disagrees with the BZ theory but is consistent both with the modified BZ length [Eq. (8)], and with the nucleation length [Eq. (10)] in the absence of detachment. However, Eq. (8) predicts a prefactor that is one order of magnitude too large. This is not surprising, since Eq. (8) was derived for steps close to thermal equilibrium;[9] under growth conditions the kink density is much larger than its equilibrium value.

Including detachment and using the lower bound $x_s = \exp(E_{BB}/2k_B T)$ as an approximation for the diffusion length yields an upper bound for the nucleation length. Expressions (10) and (12) thus give lower and upper bounds for the nucleation length, which differ approximately by a factor of 2. The lower bound [Eq. (10)] is seen to quantitatively describe the simulation data for model II, which shows that for model II the detachment may be neglected. This confirms that one-dimensional nucleation is the relevant wavelength selection mechanism under conditions of facile edge diffusion, in accordance with the conclusions from previous experimental[5] and simulational[7,8] work on surfaces vicinal to Cu(100).

However, the meander wavelength by itself does not uniquely specify the instability mechanism. The BZ theory predicts a band of unstable wavelengths extending over the interval (λ_{min}, ∞), where $\lambda_{min} = \lambda_{BZ}/\sqrt{2}$ and λ_{BZ}, as given by Eq. (5), is the wavelength of perturbations with the maximal growth rate. Numerical studies of a nonlinear evolution equation for the in-phase meander show that initial wavelengths between λ_{min} and $\lambda_{max} \approx 3\lambda_{BZ}$ are preserved during growth.[17] Thus deviations from the BZ prediction [Eq. (5)] can be attributed partly to a wavelength different from λ_{BZ} which dominates the spectrum of initial perturbations. In this context it is important to note that, for small fluxes, the wavelength measured for model II is *smaller* than the minimal unstable wavelength λ_{min} of BZ theory; this can be seen by shifting the short-dashed line in Fig. 4, which represents λ_{BZ} for model II, downward by a factor of $\sqrt{2}$. This proves that for model II an instability mechanism different from the BZ mechanism—the KESE—is the cause of the meander.

B. Crossover between the two mechanisms

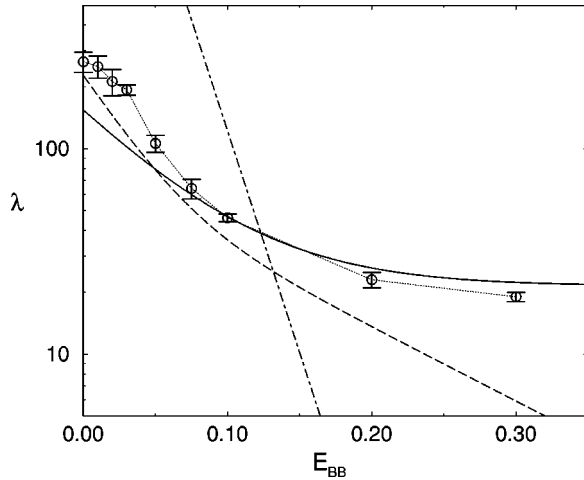Which of the two meander mechanisms is operative depends on the importance of step edge diffusion and on the

FIG. 5. The observed wavelengths (circles) for various values of the bond-breaking barrier E_{BB}. The full line is the nucleation length [Eq. (12)], the dashed line the BZ length [Eq. (5)], and the dot-dashed line the meander wavelength [Eq. (13)] for weak KESE. The crossover between the two meander mechanisms occurs around $E_{BB} \approx 0.05$ eV. Each point is an average over five independent runs on a $250 \ldots 1500 \times 30$ lattice with three steps (step spacing $l = 10$).

strength of the KESE barrier. In our SOS model both are controlled by the bond breaking barrier E_{BB}. Thus decreasing E_{BB} should lead to a crossover from the KESE instability to the BZ instability.

Simulation results for various values of E_{BB} are shown in Fig. 5. The wavelength was determined by counting the number of minima in the step profile on a finite sample. Reported wavelengths are averages over five independent runs and the error bars are the standard deviations. Since the bond breaking barrier enters the kink energy through Eq. (4), the predicted length scales [Eqs. (5) and (12)] both increase with decreasing E_{BB} in a qualitatively similar manner. In addition, the decrease of the KESE barrier implies a transition from the strong KESE regime to the weak KESE regime. The numerical data clearly show that for $E_{BB} > 0.10$ eV the meander wavelength is set by the nucleation length l_D, while for $E_{BB} < 0.05$ eV the simulations are consistent only with the BZ length, because the nucleation length is considerably smaller, and the weak KESE length [Eq. (13)] is much larger than the actual meander wavelength.

C. Variation of the ES barrier

As a further test of BZ prediction (5) we have measured the meander wavelength in model I for different values of the ES barrier. At $T = 375$ K and with the barrier $E_{ES} = 0.15$ eV used above, the Schwoebel length $l_- \approx 104 \gg l$ and $l_+ = 1$, so that $f_S \approx 1$ in Eq. (5). To study the effect of a finite ES length we carried out simulations with a single terrace[31] of width $l = 15$, varying the ES barrier between $E_{ES} = 0.06$ and 0.20 eV ($l_- = 6 - 487$), while keeping the other barriers at the values given previously. Again, the average wavelengths were calculated from five independent
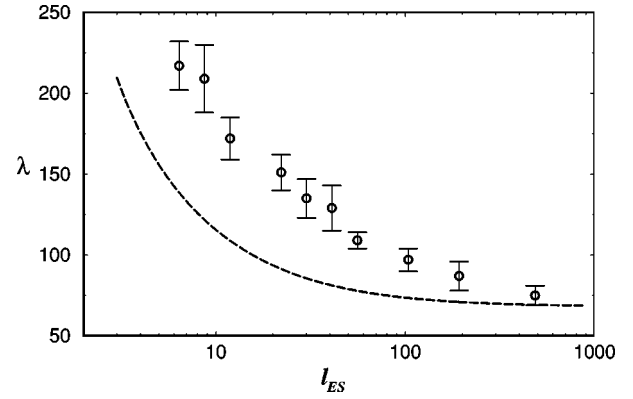

FIG. 6. Meander wavelength as a function of the ES length $l_{ES} = D/k_-$ for model I at $F = 0.25$ ML/s. Each symbol is an average over five runs on a lattice of size 1250×15 containing a single step (step spacing $l = 15$). The dashed line shows the BZ prediction [Eq. (5)].

runs. Figure 6 shows that the dependence of the meander wavelength on the ES barrier is qualitatively described by BZ theory, but Eq. (5) is not quantitatively accurate. The true ES length appears to be smaller than that given in Eq. (7) by about a factor $1/4$, which corresponds to a reduction of the ES barrier by 0.04 eV. This cannot be a simple effect of step roughness, since the implementation of the ES barrier used in the present work in fact implies that the approach to a kinked step involves a *higher* barrier than to a straight step. This issue deserves further consideration.

D. Temporal evolution

The two models can be distinguished with regard to the dynamics of meander formation. For model I the steps meander in phase from the beginning, whereas for model II the meander starts with random phase shifts between the steps (compare the early time configurations in Figs. 1 and 2). Later on, as the meander amplitude grows and the step-step interaction through the diffusion field becomes effective, the correlations between the steps grow, leading asymptotically to an in-phase step train. In light of the two different mechanisms these observations are easy to understand: Since for model I the meander is due to the BZ instability, the step train is expected to be in phase from the beginning, this being the fastest growing mode;[23] for model II the meander starts independently at each step since the meander is due to the local adatom dynamics at the step edge.

We turn next to the time evolution of the meander amplitude, which also differs for the two models (Fig.7). We consider the step width w defined by

$$w^2 \equiv L^{-1} \sum_{x=1}^{L} [y(x)]^2, \qquad (14)$$

where the x coordinate is directed along the step, L is the step length, and $y(x)$ is the step position relative to its mean. For model II, $w(t)$ increases very rapidly at the beginning, but asymptotically saturates.[33] In contrast, for model I the step width was found to increase linearly in time for the longest
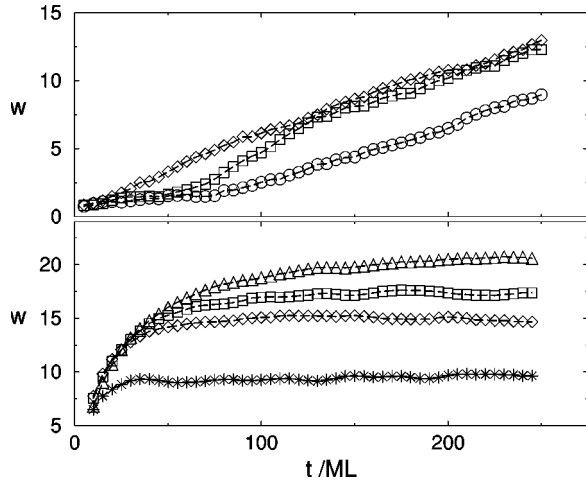
FIG. 7. Average step width w as a function of time for model I [upper panel, $F=0.1$ ($\bigcirc$), 0.4 ($\square$), and 0.8 ($\diamond$) ML/s] and model II [lower panel; $F=0.05$ ($\star$), 0.2 ($\diamond$), 0.4 ($\square$), and 0.8 ($\triangle$) ML/s], from single runs on a lattice of size 500×30 with five steps.

times we could access.[32] Both observations are at variance with the predictions of a nonlinear step evolution equation for the in-phase meander,[16–18] which predicts that $w \sim \sqrt{t}$.

Our results also contradict earlier Monte Carlo simulation,[16] in which the steps were described by single valued functions, thus prohibiting step overhangs and voids, and nucleation on the terraces was not allowed for. In these simulations a regime with $w \sim \sqrt{t}$ was observed at long times. A direct comparison of the two sets of simulations is not possible, however, because of the rather different choice of parameters. In the earlier work of Ref. 16, the concentration of adatoms was set to a value $c_{eq}^0 = 0.119$, which is several orders of magnitude larger than in our simulations. In fact, at such high adatom concentrations step flow is hardly possible, if the nucleation on the terraces is not artificially suppressed. For this reason we cannot reproduce the conditions used in the earlier simulations.[16]

The linear amplitude growth in model I suggests that minima and maxima of the step meander move at different velocities. This may be due to diffusional screening, which prevents adatoms from reaching the narrow fjords separating the cells in the upper panel of Fig. 3. In model II the fjords are wider, because adatoms are able to fill them up through edge diffusion. The saturation of the amplitude in model II may be related to the stabilizing character of the KESE step current at large slopes.[10,12]

V. RELATION TO EXPERIMENTS ON CU(100)

In this section we briefly comment on the relevance of our work for the experimentally observed meander instability[6] on surfaces vicinal to Cu(100). In these experiments two different vicinal surfaces were considered, which consist of dense-packed $\langle 110 \rangle$ steps and open $\langle 100 \rangle$ steps, respectively.

For the dense-packed $\langle 110 \rangle$ steps, edge diffusion is much more facile than detachment, so the scenario of our model II should apply. Indeed, using expression (10) for the one-dimensional nucleation length to interpret the experimentally

measured activation energy $E_a = 0.092$ eV of the meander wavelength $\lambda \sim e^{-E_a/k_BT}$, one obtains an energy barrier $E_{st} = 4E_a = 0.37$ eV for diffusion along a straight edge, which is consistent with the estimate $E_{st} = 0.45 \pm 0.08$ eV derived from the analysis of time-dependent scanning tunneling microscopy observations.[34] Also the flux dependence of (10) as $F^{-1/4}$ agrees with the experimental power law exponent of -0.21 ± 0.08.

What is missing to complete the picture is some direct experimental evidence for a (strong) KESE at the $\langle 110 \rangle$ step.[35] Here we want to point out that indirect evidence of a kink ES barrier follows from a comparison of the growth experiments[6] with step fluctuation measurements. Using the accepted value[36] $E_K \approx 0.13$ eV for the kink energy, the measurement of the prefactor of the temporal step correlation function[37] yields the estimate $E_\sigma \approx 0.91$ eV for the activation energy of the step-edge mobility σ_{st}. It was mentioned above in Sec. III that, in the absence of a strong KESE, this can be identified with the energy barrier E_{det} for the detachment of a step adatom from a kink. In a simple bond-counting approximation (which is supported by effective-medium[38] and embedded-atom[39] calculations) the detachment barrier is given by $E_{det} \approx E_{st} + 2E_K$. Using the value of E_{st} determined from the meander wavelength of the $\langle 110 \rangle$ step, this yields $E_{det} \approx 0.63$ eV, which is much smaller than the step fluctuation estimate of E_σ.

The discrepancy strongly suggests that the migration of atoms along the kinked step is suppressed by an additional kink ES barrier E_{KES}. The quantitative analysis[27] shows that for $E_{KES} > E_K$, the activation energy for σ_{st} is given by $E_\sigma = E_{det} + E_{KES} - E_K$, which, using the numbers quoted above, yields the estimate $E_{KES} \approx 0.41$ eV. In agreement with semi-empirical calculations,[38,39] the additional kink barrier is found to be comparable to the barrier E_{st} for diffusion along a straight step.

The situation is rather different for the open $\langle 100 \rangle$ step, at which a meander instability with similar characteristics has been observed.[6] Maroutian *et al.* identified the measured wavelength for the open step with the one-dimensional nucleation length (10). This interpretation seems questionable for the following two reasons. First, since the open step can be viewed as being composed entirely of $\langle 110 \rangle$ kinks, the edge diffusion barrier E_{st} is expected to be much larger than along the close-packed step,[40] while the additional barrier for detachment from a kink (which is related to the energy of $\langle 100 \rangle$ kinks) is much smaller.[39] Under these conditions the initial growth of the step is not well described by the picture of one-dimensional nucleation. Second, symmetry arguments[10,12] show that the step-edge current induced by the KESE should *stabilize*, rather than destabilize the open step. Thus the mechanism which could lead to an instability on the scale of the nucleation length is absent.

This leaves the BZ instability as the most plausible instability mechanism.[41] However, neither the activation energy (as estimated from known energetic parameters[36,38,39]) nor the $F^{-1/2}$ dependence predicted by Eq. (5) matches the experimentally determined meander wavelength.[5,6] In addition, in KMC simulations of Cu(100), the surface composed of

$\langle 100 \rangle$ steps was found to be stable;[7] possibly this reflects the stabilizing KESE. The experimentally observed instability of the open step thus poses a major puzzle at the moment.

VI. CONCLUSION

In summary, we have studied the unstable growth dynamics of vicinal surfaces using a SOS model with two different choices of atomic processes. It was shown that in both cases the steps form an in-phase wave pattern. The formation mechanism and the wavelength of the pattern depends on whether the diffusion of adatoms along the step edges is significant or not. In the case where step edge diffusion is negligible the wavelength was found to be correctly predicted by the continuum theory of BZ, while in the case of facile edge diffusion (combined with an ES barrier at kinks) it is set by the one-dimensional nucleation length.

In both cases good agreement between the KMC simulations and the analytical predictions [Eqs. (5) and (10)] for the meander wavelength was achieved *without any adjustable parameters*. However, the asymptotic time evolution of the step profile disagrees with the prediction of an effective step evolution equation.[16–18] Whether this disagreement is due to different physics described by the continuum and discrete models or due to the approximations made deriving the step equation remains to be clarified.

[1] L. Schwenger, R.L. Folkerts, and H.-J. Ernst, Phys. Rev. B **55**, R7406 (1997); J.E. Van Nostrand, S.J. Chey, and D.G. Cahill, *ibid.* **57**, 12 536 (1998); P. Tejedor, P. Šmilauer, and B.A. Joyce, Microelectron. J. **30**, 477 (1999).

[2] M. Rost, P. Šmilauer, and J. Krug, Surf. Sci. **369**, 393 (1996).

[3] G.S. Bales and A. Zangwill, Phys. Rev. B **41**, 5500 (1990).

[4] G. Ehrlich and F.G. Hudda, J. Chem. Phys. **44**, 1039 (1966); R.L. Schwoebel and E.J. Shipsey, J. Appl. Phys. **37**, 3682 (1966).

[5] T. Maroutian, L. Douillard, and H.-J. Ernst, Phys. Rev. Lett. **83**, 4353 (1999).

[6] T. Maroutian, L. Douillard, and H.-J. Ernst, Phys. Rev. B **64**, 165401 (2001).

[7] M. Rusanen, I.T. Koponen, J. Heinonen, and T. Ala-Nissila, Phys. Rev. Lett. **86**, 5317 (2001).

[8] M. Rusanen, I.T. Koponen, T. Ala-Nissila, C. Ghosh, and T.S. Rahman, Phys. Rev. B **65**, 041404(R) (2002).

[9] O. Pierre-Louis, Phys. Rev. Lett. **87**, 106104 (2001).

[10] O. Pierre-Louis, M.R. D'Orsogna, and T.L. Einstein, Phys. Rev. Lett. **82**, 3661 (1999).

[11] M.V. Ramana Murty and B.H. Cooper, Phys. Rev. Lett. **83**, 352 (1999).

[12] P. Politi and J. Krug, Surf. Sci. **446**, 89 (2000).

[13] P. Politi and J. Villain, Phys. Rev. B **54**, 5114 (1996).

[14] J. Krug, Adv. Phys. **46**, 139 (1997).

[15] P. Politi, G. Grenet, A. Marty, A. Ponchet, and J. Villain, Phys. Rep. **324**, 271 (2000).

[16] O. Pierre-Louis, C. Misbah, Y. Saito, J. Krug, and P. Politi, Phys. Rev. Lett. **80**, 4221 (1998).

[17] J. Kallunki and J. Krug, Phys. Rev. E **62**, 6229 (2000).

[18] F. Gillet, O. Pierre-Louis, and C. Misbah, Eur. Phys. J. B **18**, 519 (2000).

[19] M. Kotrla, Comput. Phys. Commun. **97**, 82 (1996).

[20] P. Šmilauer and D.D. Vvedensky, Phys. Rev. B **52**, 14 263 (1995).

[21] M. Siegert and M. Plischke, Phys. Rev. E **53**, 307 (1996).

[22] P. Šmilauer, M.R. Wilby, and D.D. Vvedensky, Phys. Rev. B **48**, 4968 (1993).

[23] A. Pimpinelli, I. Elkinani, A. Karma, C. Misbah, and J. Villain, J. Phys.: Condens. Matter **6**, 2661 (1994).

[24] H.-C. Jeong and E.D. Williams, Surf. Sci. Rep. **34**, 171 (1999).

[25] J. Krug, H.T. Dobbs, and S. Majaniemi, Z. Phys. B: Condens. Matter **97**, 281 (1995).

[26] A. Pimpinelli, J. Villain, and D.E. Wolf, J. Phys. I **3**, 447 (1993).

[27] J. Kallunki and J. Krug (unpublished).

[28] R. Ghez and S.S. Iyer, IBM J. Res. Dev. **32**, 804 (1988).

[29] P. Politi, J. Phys. I **7**, 797 (1997); J. Krug and M. Schimschak, *ibid.* **5**, 1065 (1995).

[30] P. Jensen, H. Larralde, and A. Pimpinelli, Phys. Rev. B **55**, 2556 (1997).

[31] Because of the periodic boundary conditions, a single terrace is equivalent to an infinite step train with steps that are perfectly in phase.

[32] At times longer than those depicted in Fig. 7, step flow breaks down due to the formation of step loops and craters, and a transition to mound growth sets in Ref. 2. The details of this process will be addressed elsewhere.

[33] In a recent KMC simulation (Ref. 8) of Cu(100), where step meandering was also attributed to the KESE, $w \sim t^{0.3}$ was observed at early times ($t < 5$ ML). In earlier SOS model simulations (Ref. 10) the behavior $w \sim t^{0.3}$ and $w \sim t^{0.57}$ was reported for weak and strong KESE's, respectively.

[34] M. Giesen-Seibert and H. Ibach, Surf. Sci. **316**, 205 (1994).

[35] The direct observation of an additional barrier for corner rounding was reported for Rh(100); see G.L. Kellogg, Surf. Sci. **359**, 237 (1996).

[36] M. Giesen, Prog. Surf. Sci. **68**, 1 (2001).

[37] M. Giesen-Seibert, F. Schmitz, R. Jentjens, and H. Ibach, Surf. Sci. **329**, 47 (1995).

[38] J. Merikoski, I. Vattulainen, J. Heinonen, and T. Ala-Nissila, Surf. Sci. **387**, 167 (1997).

[39] H. Mehl, O. Biham, I. Furman, and M. Karimi, Phys. Rev. B **60**, 2106 (1999).

[40] O.S. Trushin, K. Kokko, P.T. Salo, W. Hergert, and M. Kotrla, Phys. Rev. B **56**, 12 135 (1997).

[41] T. Maroutian, Ph.D. thesis, Université Paris 7-Denis Diderot, 2001.